Designation: E2860 – 12

Standard Test Method for Residual Stress Measurement by X-Ray Diffraction for Bearing Steels[1]

This standard is issued under the fixed designation E2860; the number immediately following the designation indicates the year of original adoption or, in the case of revision, the year of last revision. A number in parentheses indicates the year of last reapproval. A superscript epsilon (ε) indicates an editorial change since the last revision or reapproval.

INTRODUCTION

The measurement of residual stress using X-ray diffraction (XRD) techniques has gained much popularity in the materials testing field over the past half century and has become a mandatory test for many production and prototype bearing components. However, measurement practices have evolved over this time period. With each evolutionary step, it was discovered that previous assumptions were sometimes erroneous, and as such, results obtained were less reliable than those obtained using state-of-the-art XRD techniques. Equipment and procedures used today often reflect different periods in this evolution; for example, systems that still use the single- and double-exposure techniques as well as others that use more advanced multiple exposure techniques can all currently be found in widespread use. Moreover, many assumptions made, such as negligible shear components and non-oscillatory $\sin^2\psi$ distributions, cannot safely be made for bearing materials in which the demand for measurement accuracy is high. The use of the most current techniques is, therefore, mandatory to achieve not only the most reliable measurement results but also to enable identification and evaluation of potential measurement errors, thus paving the way for future developments.

1. Scope

1.1 This test method covers a procedure for experimentally determining macroscopic residual stress tensor components of quasi-isotropic bearing steel materials by X-ray diffraction (XRD).

1.2 This test method provides a guide for experimentally determining stress values, which play a significant role in bearing life.

1.3 Examples of how tensor values are used are:

1.3.1 Detection of grinding type and abusive grinding;

1.3.2 Determination of tool wear in turning operations;

1.3.3 Monitoring of carburizing and nitriding residual stress effects;

1.3.4 Monitoring effects of surface treatments such as sand blasting, shot peening, and honing;

1.3.5 Tracking of component life and rolling contact fatigue effects;

1.3.6 Failure analysis;

1.3.7 Relaxation of residual stress; and

1.3.8 Other residual-stress-related issues that potentially affect bearings.

1.4 *Units*—The values stated in SI units are to be regarded as standard. No other units of measurement are included in this standard.

1.5 *This standard does not purport to address all of the safety concerns, if any, associated with its use. It is the responsibility of the user of this standard to establish appropriate safety and health practices and determine the applicability of regulatory limitations prior to use.*

2. Referenced Documents

2.1 *ASTM Standards:*[2]

E6 Terminology Relating to Methods of Mechanical Testing

E7 Terminology Relating to Metallography

E915 Test Method for Verifying the Alignment of X-Ray Diffraction Instrumentation for Residual Stress Measurement

E1426 Test Method for Determining the Effective Elastic Parameter for X-Ray Diffraction Measurements of Residual Stress

[1] This test method is under the jurisdiction of ASTM Committee E28 on Mechanical Testing and is the direct responsibility of Subcommittee E28.13 on Residual Stress Measurement.

Current edition approved April 1, 2012. Published May 2012. DOI: 10.1520/E2860–12.

[2] For referenced ASTM standards, visit the ASTM website, www.astm.org, or contact ASTM Customer Service at service@astm.org. For *Annual Book of ASTM Standards* volume information, refer to the standard's Document Summary page on the ASTM website.

Copyright © ASTM International, 100 Barr Harbor Drive, PO Box C700, West Conshohocken, PA 19428-2959. United States

2.2 *ANSI Standards:*[3]

N43.2 Radiation Safety for X-ray Diffraction and Fluorescence Analysis Equipment

N43.3 For General Radiation Safety—Installations Using Non-Medical X-Ray and Sealed Gamma-Ray Sources, Energies Up to 10 MeV

3. Terminology

3.1 *Definitions*—Many of the terms used in this test method are defined in Terminologies E6 and E7.

3.2 *Definitions of Terms Specific to This Standard:*

3.2.1 *interplanar spacing, n*—perpendicular distance between adjacent parallel atomic planes.

3.2.2 *macrostress, n*—average stress acting over a region of the test specimen containing many gains/crystals/coherent domains.

3.3 *Abbreviations:*

3.3.1 *ALARA*—As low as reasonably achievable

3.3.2 *FWHM*—Full width half maximum

3.3.3 *LPA*—Lorentz-polarization-absorption

3.3.4 *MSDS*—Material safety data sheet

3.3.5 *XEC*—X-ray elastic constant

3.3.6 *XRD*—X-ray diffraction

3.4 *Symbols:*

$\frac{1}{2} S_2^{\{hkl\}}$ = X-ray elastic constant of quasi-isotropic material equal to $\frac{1+\nu}{E_{eff}^{\{hkl\}}}$

α_L = Linear thermal expansion coefficient

β = Angle between the incident beam and σ_{33} or surface normal on the σ_{33} σ_{11} plane

χ = Angle between the $\sigma_{\varphi+90°}$ direction and the normal to the diffracting plane

χ_m = Fixed χ offset used in modified-chi mode

d = Interplanar spacing between crystallographic planes; also called *d*-spacing

d_o = Interplanar spacing for unstressed material

$d_\perp$ = Perpendicular spacing

Δd = Change in interplanar spacing caused by stress

ε_{ij} = Strain component *i*, *j*

E = Modulus of elasticity (Young's modulus)

$E_{eff}^{\{hkl\}}$ = Effective elastic modulus for X-ray measurements

μ = Attenuation coefficient

η = Rotation of the sample around the measuring direction given by φ and ψ or χ and β

ω or Ω = Angle between the specimen surface and incident beam when $\chi = 0°$

φ = Angle between the σ_{11} direction and measurement direction azimuth, see Fig. 1

"*hkl*" = Miller indices

σ_{ij} = Normal stress component *i*, *j*

$s_1^{\{hkl\}}$ = X-ray elastic constant of quasi-isotropic material equal to $\frac{-\nu}{E_{eff}^{\{hkl\}}}$

τ_{ij} = Shear stress component *i*, *j*

θ = Bragg angle

ν = Poisson's ratio

x^{Mode} = Mode dependent depth of penetration

ψ = Angle between the specimen surface normal and the scattering vector, that is, normal to the diffracting plane, see Fig. 1

4. Summary of Test Method

4.1 A test specimen is placed in a XRD goniometer aligned as per Test Method E915.

4.2 The diffraction profile is collected over three or more angles within the required angular range for a given {hkl} plane, although at least seven or more are recommended.

4.3 The XRD profile data are then corrected for LPA, background, and instrument-specific corrections.

4.4 The peak position/Bragg angle is determined for each XRD peak profile.

4.5 The *d*-spacings are calculated from the peak positions via Bragg's law.

4.6 The *d*-spacing values are plotted versus their $\sin^2\psi$ or $\sin^2\beta$ values, and the residual stress is calculated using Eq 4 or Eq 8, respectively.

4.7 The error in measurement is evaluated as per Section 14.

4.8 The following additional corrections may be applied. The use of these corrections shall be clearly indicated with the reported results.

4.8.1 Depth of penetration correction (see 12.12) and

4.8.2 Relaxation as a result of material removal correction (see 12.14).

[3] Available from American National Standards Institute (ANSI), 25 W. 43rd St., 4th Floor, New York, NY 10036, http://www.ansi.org.

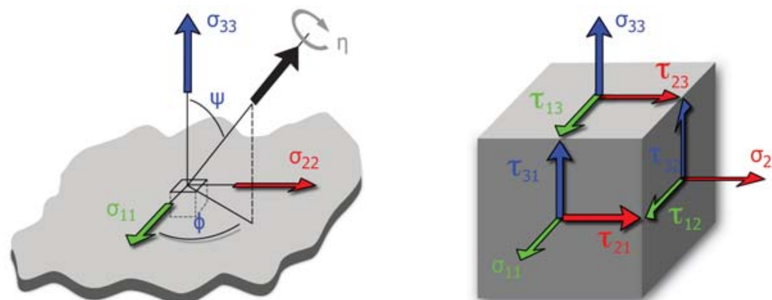

FIG. 1 Stress Tensor Components

5. Significance and Use

5.1 This test method covers a procedure for experimentally determining macroscopic residual stress tensor components of quasi-isotropic bearing steel materials by XRD. Here the stress components are represented by the tensor σ_{ij} as shown in Eq 1 (**1**,[4] p. 40). The stress strain relationship in any direction of a component is defined by Eq 2 with respect to the azimuth phi(φ) and polar angle psi(ψ) defined in Fig. 1 (**1**, p. 132).

$$\sigma_{ij} = \begin{bmatrix} \sigma_{11} & \tau_{12} & \tau_{13} \\ \tau_{21} & \sigma_{22} & \tau_{23} \\ \tau_{31} & \tau_{32} & \sigma_{33} \end{bmatrix} \quad \text{where } \tau_{ij} = \tau_{ji} \tag{1}$$

$$\varepsilon_{\varphi\psi}^{\{hkl\}} = \frac{1}{2}s_2^{\{hkl\}}\left[\sigma_{11}\cos^2\varphi\,\sin^2\psi + \sigma_{22}\sin^2\varphi\,\sin^2\psi + \sigma_{33}\cos^2\psi\right] + \frac{1}{2}s_2^{\{hkl\}}\left[\tau_{12}\sin(2\varphi)\,\sin^2\psi + \tau_{13}\cos\varphi\sin(2\psi) + \tau_{23}\sin\varphi\sin(2\psi)\right] + s_1^{\{hkl\}}\left[\sigma_{11} + \sigma_{22} + \sigma_{33}\right] \tag{2}$$

5.1.1 Alternatively, Eq 2 may also be shown in the following arrangement (**2**, p. 126):

$$\varepsilon_{\varphi\psi}^{\{hkl\}} = \frac{1}{2}s_2^{\{hkl\}}\left[\sigma_{11}\cos^2\varphi + \tau_{12}\sin(2\varphi) + \sigma_{22}\sin^2\varphi - \sigma_{33}\right]\sin^2\psi + \frac{1}{2}s_2^{\{hkl\}}\sigma_{33} - s_1^{\{hkl\}}\left[\sigma_{11} + \sigma_{22} + \sigma_{33}\right] + \frac{1}{2}s_2^{\{hkl\}}\left[\tau_{13}\cos\varphi + \tau_{23}\sin\varphi\right]\sin(2\psi)$$

[4] The boldface numbers in parentheses refer to the list of references at the end of this standard.

5.2 Using XRD and Bragg's law, interplanar strain measurements are performed for multiple orientations. The orientations are selected based on a modified version of Eq 2, which is dictated by the mode used. Conflicting nomenclature may be found in literature with regard to mode names. For example, what may be referred to as a ψ (psi) diffractometer in Europe may be called a χ (chi) diffractometer in North America. The three modes considered here will be referred to as omega, chi, and modified-chi as described in 9.5.

5.3 *Omega Mode (Iso Inclination) and Chi Mode (Side Inclination)*—Interplanar strain measurements are performed at multiple ψ angles along one φ azimuth (let φ = 0°) (Figs. 2 and 3), reducing Eq 2 to Eq 3. Stress normal to the surface (σ_{33}) is assumed to be insignificant because of the shallow depth of penetration of X-rays at the free surface, reducing Eq 3 to Eq 4. Post-measurement corrections may be applied to account for possible σ_{33} influences (12.12). Since the σ_{ij} values will remain constant for a given azimuth, the $s_1^{\{hkl\}}$ term is renamed *C*.

$$\varepsilon_{\varphi\psi}^{\{hkl\}} = \frac{1}{2}s_2^{\{hkl\}}\left[\sigma_{11}\sin^2\psi + \sigma_{33}\cos^2\psi\right] + \frac{1}{2}s_2^{\{hkl\}}\left[\tau_{13}\sin(2\psi)\right] + s_1^{\{hkl\}}\left[\sigma_{11} + \sigma_{22} + \sigma_{33}\right] \tag{3}$$

$$\varepsilon_{\varphi\psi}^{\{hkl\}} = \frac{1}{2}s_2^{\{hkl\}}\left[\sigma_{11}\sin^2\psi + \tau_{13}\sin(2\psi)\right] + C \tag{4}$$

5.3.1 The measured interplanar spacing values are converted to strain using Eq 24, Eq 25, or Eq 26. Eq 4 is used to fit the strain versus $\sin^2\psi$ data yielding the values σ_{11}, τ_{13}, and *C*. The measurement can then be repeated for multiple phi angles (for example 0, 45, and 90°) to determine the full

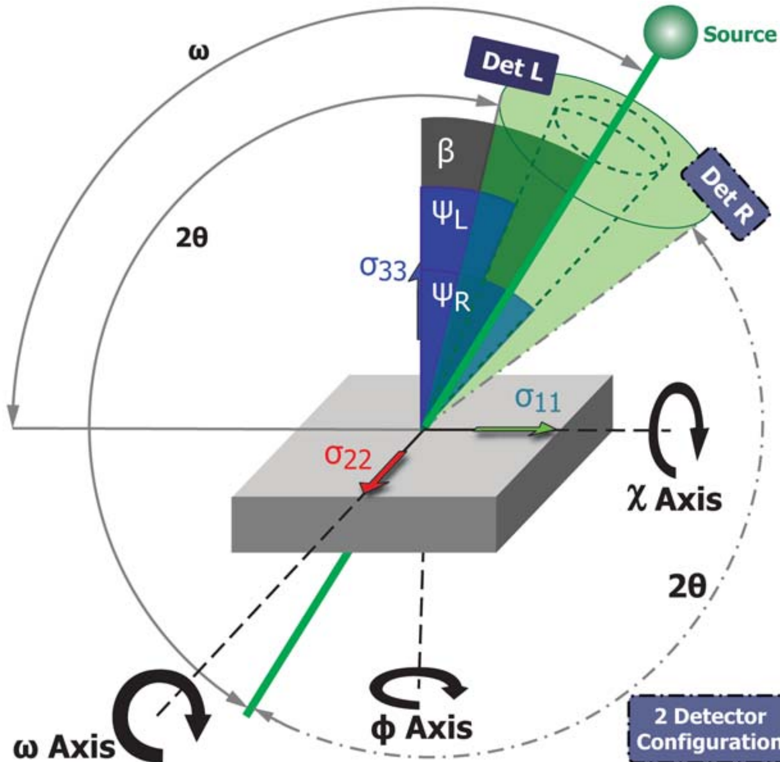

FIG. 2 Omega Mode Diagram for Measurement in σ_{11} Direction

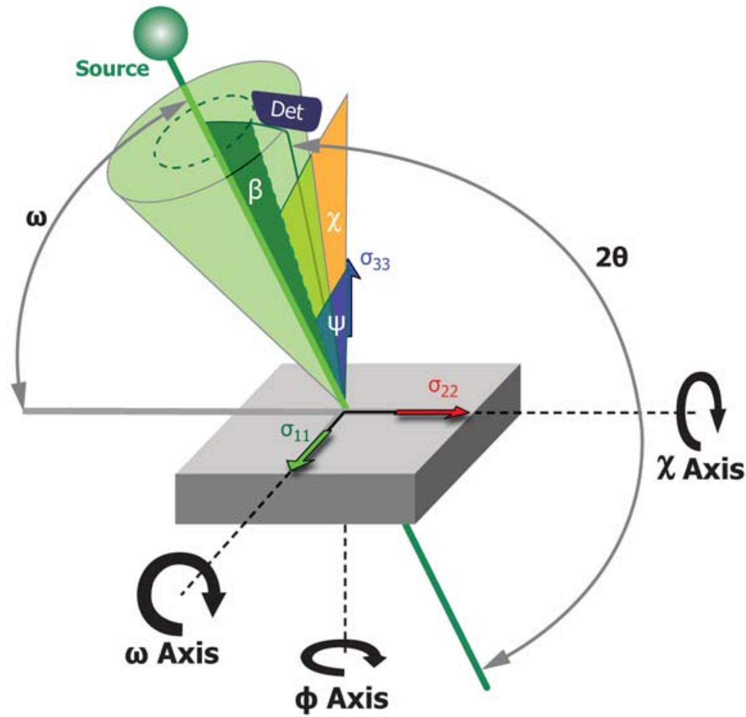

NOTE 1—Stress matrix is rotated 90° about the surface normal compared to Fig. 2 and Fig. 14.

FIG. 3 Chi Mode Diagram for Measurement in σ_{11} Direction

stress/strain tensor. The value, σ_{11}, will influence the overall slope of the data, while τ_{13} is related to the direction and degree of elliptical opening. Fig. 4 shows a simulated *d* versus $\sin^2\psi$ profile for the tensor shown. Here the positive 20-MPa τ_{13} stress results in an elliptical opening in which the positive psi range opens upward and the negative psi range opens downward. A higher τ_{13} value will cause a larger elliptical opening. A negative 20-MPa τ_{13} stress would result in the same elliptical opening only the direction would be reversed with the positive psi range opening downwards and the negative psi range opening upwards as shown in Fig. 5.

5.4 *Modified Chi Mode*—Interplanar strain measurements are performed at multiple β angles with a fixed χ offset, χ_m (Fig. 6). Measurements at various β angles do not provide a constant φ angle (Fig. 7), therefore, Eq 2 cannot be simplified in the same manner as for omega and chi mode.

5.4.1 Eq 2 shall be rewritten in terms of β and χ_m. Eq 5 and 6 are obtained from the solution for a right-angled spherical triangle (**3**).

$$\psi = \arccos(\cos\beta\cos\chi_m) \tag{5}$$

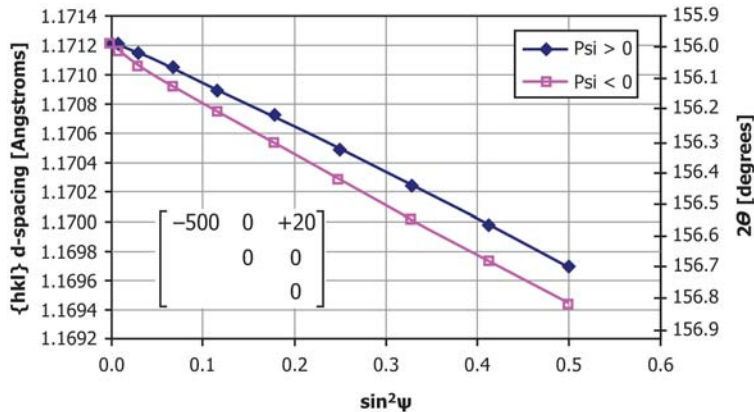

FIG. 4 Sample *d* (2θ) Versus $\sin^2\psi$ Dataset with σ_{11} = -500 MPa and τ_{13} = +20 MPa

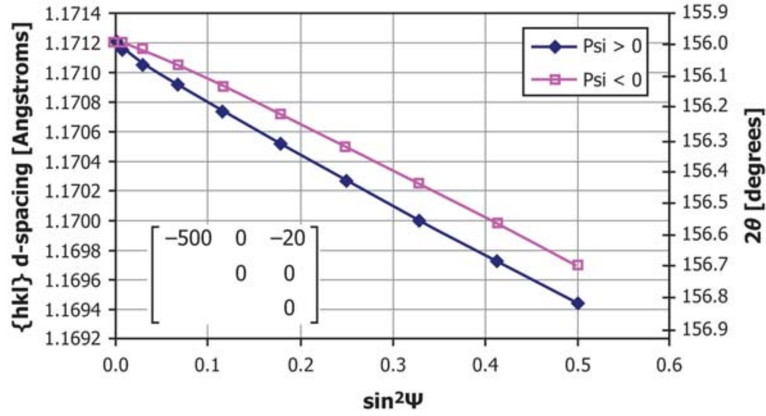

FIG. 5 Sample d (2θ) Versus $\sin^2\psi$ Dataset with σ_{11} = -500 MPa and τ_{13} = -20 MPa

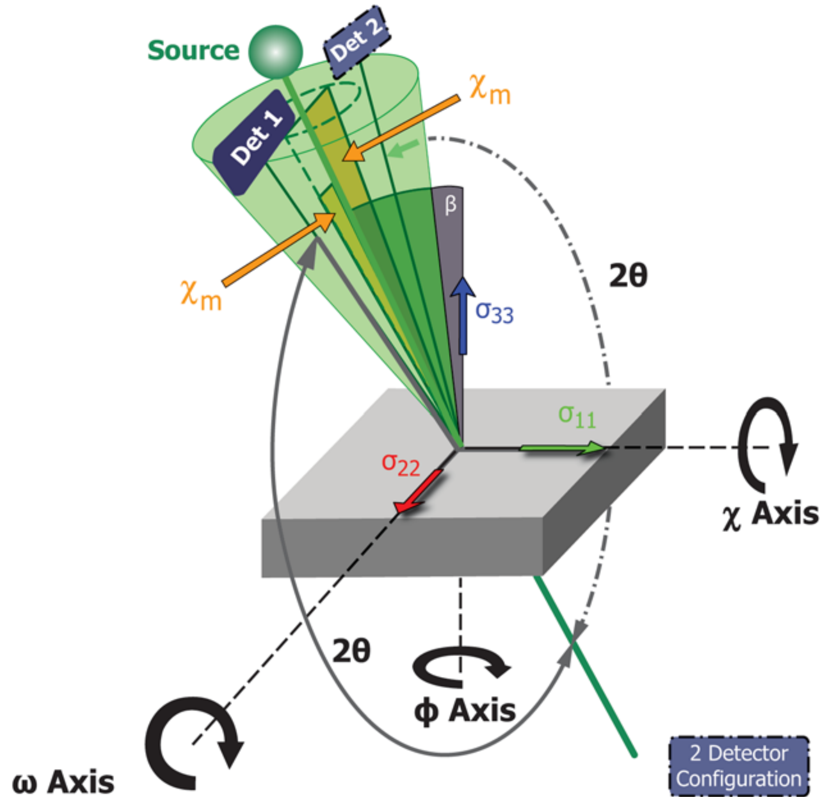

FIG. 6 Modified Chi Mode Diagram for Measurement in σ_{11} Direction

$$\varphi = \arccos\left(\frac{\sin\beta\cos\chi_m}{\sin\psi}\right) \quad (6)$$

5.4.2 Substituting φ and ψ in Eq 2 with Eq 5 and 6 (see X1.1), we get:

$$\varepsilon_{\beta\chi_m}^{\{hkl\}} = \frac{1}{2}s_2^{\{hkl\}}\left[\sigma_{11}\sin^2\beta\cos^2\chi_m + \sigma_{22}\sin^2\chi_m + \sigma_{33}\cos^2\beta\cos^2\chi_m\right]$$
$$+\frac{1}{2}s_2^{\{hkl\}}\left[\tau_{12}\sin\beta\sin(2\chi_m) + \tau_{13}\sin(2\beta)\cos^2\chi_m + \tau_{23}\cos\beta\sin(2\chi_m)\right]$$
$$+s_1^{\{hkl\}}\left[\sigma_{11}+\sigma_{22}+\sigma_{33}\right] \quad (7)$$

5.4.3 Stress normal to the surface (σ_{33}) is assumed to be insignificant because of the shallow depth of penetration of X-rays at the free surface reducing Eq 7 to Eq 8. Post-measurement corrections may be applied to account for possible σ_{33} influences (see 12.12). Since the σ_{ij} values and χ_m will remain constant for a given azimuth, the $s_1^{\{hkl\}}$ term is renamed C, and the σ_{22} term is renamed D.

$$\varepsilon_{\beta\chi_m}^{\{hkl\}} = \frac{1}{2}s_2^{\{hkl\}}\left[\sigma_{11}\sin^2\beta\cos^2\chi_m + D\right] + \frac{1}{2}s_2^{\{hkl\}}\left[\tau_{12}\sin\beta\sin(2\chi_m)\right.$$
$$\left.+\tau_{13}\sin(2\beta)\cos^2\chi_m + \tau_{23}\cos\beta\sin(2\chi_m)\right] + C \quad (8)$$

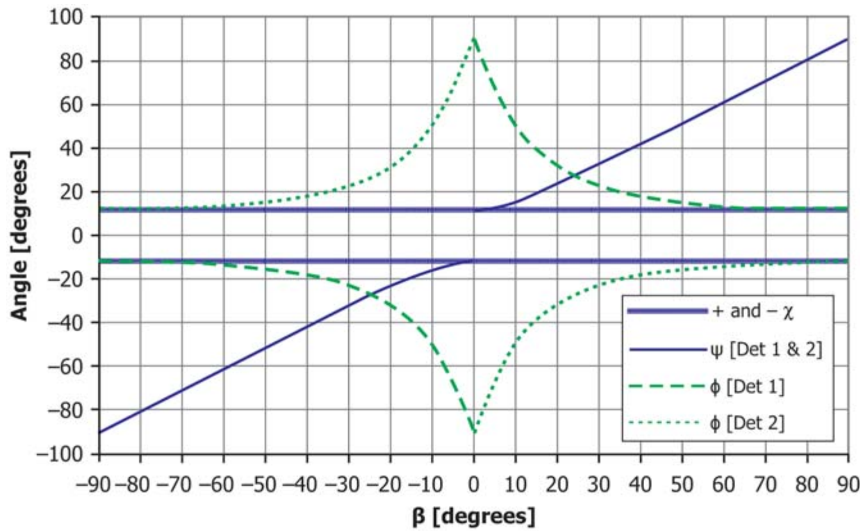

FIG. 7 ψ and φ Angles Versus β Angle for Modified Chi Mode with χ_m = 12°

5.4.4 The σ_{11} influence on the d versus $\sin^2\beta$ plot is similar to omega and chi mode (Fig. 8) with the exception that the slope shall be divided by $\cos^2\chi_m$. This increases the effective ½ $s_2^{\{hkl\}}$ by a factor of $1/\cos^2\chi_m$ for σ_{11}.

5.4.5 The τ_{ij} influences on the d versus $\sin^2\beta$ plot are more complex and are often assumed to be zero (**3**). However, this may not be true and significant errors in the calculated stress may result. Figs. 9-13 show the d versus $\sin^2\beta$ influences of individual shear components for modified chi mode considering two detector positions (χ_m = +12° and χ_m = -12°). Components τ_{12} and τ_{13} cause a symmetrical opening about the σ_{11} slope influence for either detector position (Figs. 9-11); therefore, σ_{11} can still be determined by simply averaging the positive and negative β data. Fitting the opening to the τ_{12} and τ_{13} terms may be possible, although distinguishing between the two influences through regression is not normally possible.

5.4.6 The τ_{23} value affects the d versus $\sin^2\beta$ slope in a similar fashion to σ_{11} for each detector position (Figs. 12 and 13). This is an unwanted effect since the σ_{11} and τ_{23} influence cannot be resolved for one χ_m position. In this instance, the τ_{23} shear stress of -100 MPa results in a calculated σ_{11} value of -472.5 MPa for χ_m = +12° or -527.5 MPa for χ_m = -12°, while the actual value is -500 MPa. The value, σ_{11} can still be determined by averaging the β data for both χ_m positions.

5.4.7 The use of the modified chi mode may be used to determine σ_{11} but shall be approached with caution using one χ_m position because of the possible presence of a τ_{23} stress. The combination of multiple shear stresses including τ_{23} results in increasingly complex shear influences. Chi and omega mode are preferred over modified chi for these reasons.

6. Apparatus

6.1 A typical X-ray diffractometer is composed of the following main components:

6.1.1 *Goniometer*—An angle-measuring device responsible for the positioning of the source, detectors, and sample relative to each other.

6.1.2 *X-Ray Source*—There are generally three X-ray sources used for XRD.

6.1.2.1 *Conventional Sealed Tube*—This is by far the most common found in XRD equipment. It is identified by its anode target element such as chromium (Cr), manganese (Mn), or copper (Cu). The anode is bombarded by electrons to produce specific X-ray wavelengths unique to the target element.

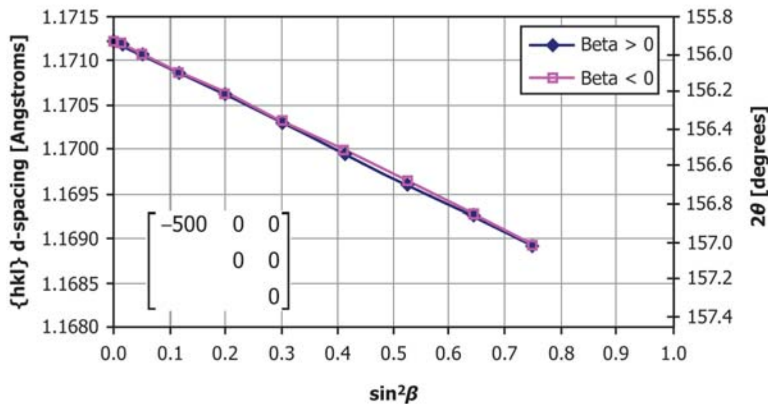

FIG. 8 Sample d (2θ) Versus $\sin^2\beta$ Dataset with σ_{11} = -500 MPa

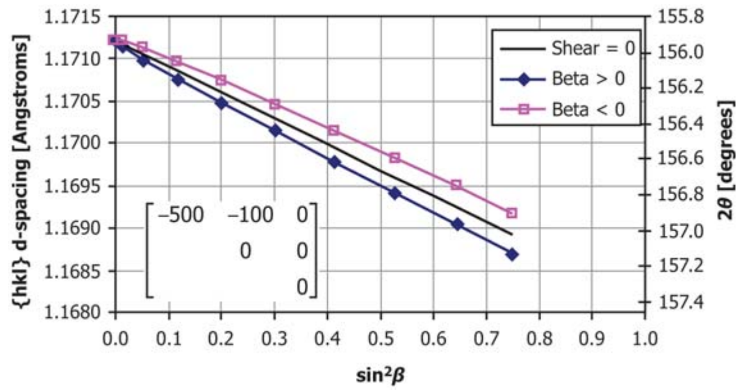

FIG. 9 Sample *d* (2θ) versus $\sin^2\beta$ Dataset with χ_m = +12°, σ_{11} = -500 MPa, and τ_{12} = -100 MPa

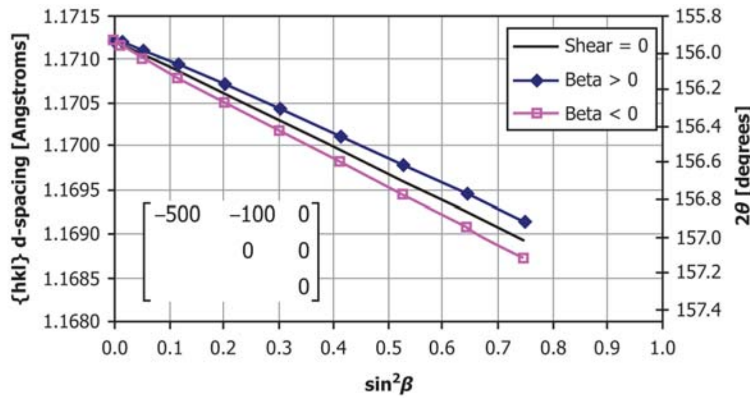

FIG. 10 Sample *d* (2θ) Versus $\sin^2\beta$ Dataset with χ_m = -12°, σ_{11} = -500 MPa, and τ_{12} = -100 MPa

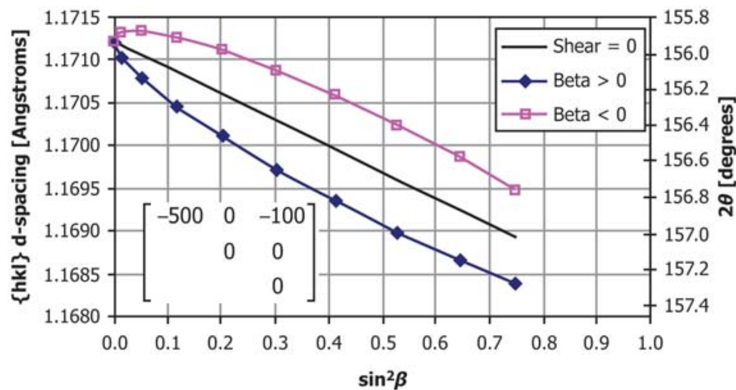

FIG. 11 Sample *d* (2θ) Versus $\sin^2\beta$ Dataset with χ_m = +12 or -12°, σ_{11} = -500 MPa, and τ_{13} = -100 MPa

6.1.2.2 *Rotating Anode Tube*—This style of tube offers a higher intensity than a conventional sealed tube.

6.1.2.3 *Synchrotron*—Particle accelerator that is capable of producing a high-intensity X-ray beam.

6.1.2.4 *Sealed Radioactive Sources*—Although not commonly used, they may be utilized.

6.1.3 *Detector*—Detectors may be of single channel, multichannel linear, or area design.

6.1.4 *Software*—Software is grouped into the following main categories:

6.1.4.1 *Goniometer control*—Responsible for positioning of the sample relative to the incident beam and detector(s) in automated goniometers.

6.1.4.2 *Data acquisition*—Responsible for the collection of diffraction profile data from the detector(s).

6.1.4.3 *Data processing*—Responsible for all data fitting and calculations.

6.1.4.4 *Data management*—Responsible for data file management as well as overall record keeping. Individual measurement data is typically stored in a file format that can later be

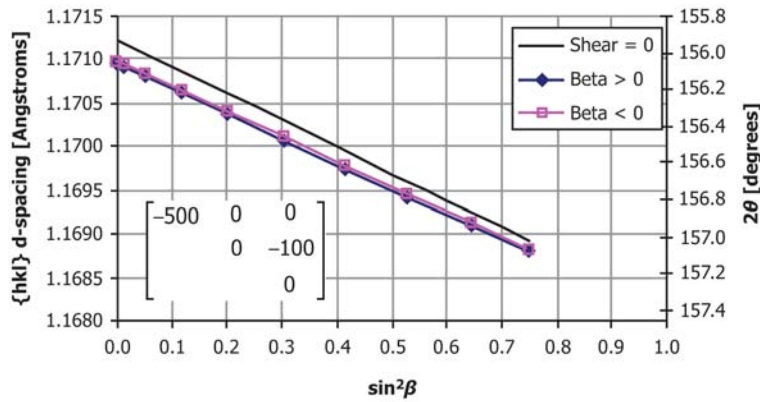

FIG. 12 Sample d (2θ) Versus $\sin^2\beta$ Dataset with χ_m = +12°, σ_{11} = -500 MPa, τ_{23} = -100 MPa, and Measured σ_{11} = -472.5 MPa

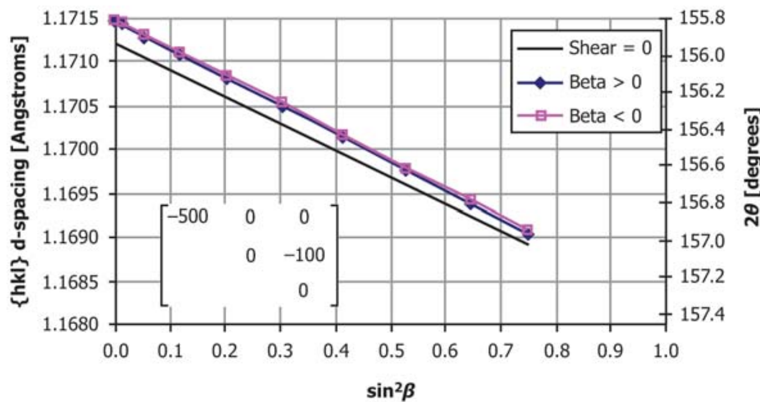

FIG. 13 Sample d (2θ) Versus $\sin^2\beta$ Dataset with χ_m = -12°, σ_{11} = -500 MPa, τ_{23} = -100 MPa, and Measured σ_{11} = -527.5 MPa

reopened for reevaluation. It is often beneficial to keep a database of key measurement values and file names.

7. Hazards

7.1 Regarding the use of analytical X-ray equipment, local government regulations or guidelines shall always be followed. Examples include ANSI N43.2-2001 and ANSI N43.3.

7.2 The as low as reasonably achievable (ALARA) philosophy should always be used when dealing with radiation exposure.

7.3 Always follow the safety guidelines of the equipment manufacturer.

7.4 Refer to material safety data sheets (MSDS) sheets for handling of dangerous materials potentially found in XRD equipment (that is, beryllium and lead).

7.5 The high voltage used to generate X-rays is very dangerous. Follow the manufacturer's and local guidelines when dealing with high-voltage equipment.

8. Test Specimens

8.1 This guide is intended for materials with the following characteristics:

8.1.1 Fine grain size and

8.1.2 Near random coherent domain orientation distribution.

8.2 Test specimens shall be clean at the measured location and should be free of visible signs of oxidation, material debris, and coatings such as oil and paint.

8.3 Sample surfaces shall be free of any significant roughness. Grooves produced by machining perpendicular to the measurement direction may affect measurement results (**4**, p. 21).

8.4 Sample surfaces may be prepared using electropolishing as this method does not impart stress within the sample; however, removal of stressed layers may influence the subsurface residual stress state. Corrections are available to estimate the true stress that existed when the specimen was intact (see 12.13).

8.5 If material removal methods other than electropolishing (that is, grinding or sanding) are necessary, subsequent electropolishing is required to ensure the cold-worked region is removed. For light grinding or sanding, the removal of 0.25 mm is recommended.

8.6 Sample curvatures should not exceed the acceptable limits for the goniometer setup used (see 9.1.2).

8.7 Measurement of a single-phase stress in multiphase materials may not be representative of the bulk material when significant amount of additional phases are present.

8.8 Measurement of thin coatings may not be representative of the bulk material. Diffraction of the substrate may create interfering diffraction lines.

9. Preparation of Apparatus

9.1 *Primary Beam Size*—The primary beam size is typically adjustable using a primary beam aperture. To ensure the best counting statistics, the largest beam size should be used that does not exceed the following limitations:

9.1.1 Preferably beam divergence should not exceed 1° (**2**, p. 107). Divergence may be limited by devices such as Soller slits and sample masking.

9.1.2 For cylindrical specimens of radius, *R*, the maximum incident X-ray spot size to use shall be R/6 for 5 % error and R/4 for 10 % error in the hoop direction and R/2.5 and R/2 for 5 % and 10 % error, respectively, in the axial direction. In cases in which the beam size cannot be sufficiently small, corrections can be applied (**5**, p. 107), (**6**, pp. 327-336).

9.2 *Target/Plane Combination*—The characteristic wavelengths available for diffraction are determined by the target element. A list of common target elements, their K line wavelengths, and K_β filters are shown in Table 1.

9.2.1 There are several possible target-plane combinations for a given bearing steel that will produce a diffraction peak. When choosing a combination, there are many factors to take into account including the relative peak versus background intensity, mass absorption coefficient, possible interfering peaks, and strain resolution. Higher 2θ values will have a higher strain resolution thus improving measurement precision. A higher mass absorption coefficient reduces the depth of penetration. Shallow penetration reduces stress gradient effects but limits the number of coherent domains contributing to the diffraction profile. When performing residual stress measurements in martensitic bearing steels, the Cr Kα target is typically used with the {211} plane with a 2θ angle of approximately 154 to 157º. When performing residual stress measurements in austenitic bearing steels, the Mn Kα target is typically used with the {311} plane with a 2θ angle of approximately 152 to 155º. Table 2 shows a list of target-plane combinations commonly shown in literature. X-Ray elastic constants ½ s_2 and s_1 may also be determined with Test Method E1426. The depth of penetration (*x*) for omega and chi mode based on Eq 9 and 10 are included (DIN En 15305, p. 22), (**1**, p. 106). Note that when ψ = 0, the depth of penetration is the same for either mode. The ψ = 0 values are, therefore, listed in the same column. The depth of penetration for modified chi mode is given by Eq 11.

TABLE 1 Target Wavelengths and Appropriate K_β Suppression Filers

Target Element	$K_{\alpha1}$	$K_{\alpha2}$	K_β	Filter K_{edge}
	[Å] = [nm × 10]			
22 Ti	2.748 51	2.752 16	2.513 91	...
24 Cr	2.289 70	2.293 606	2.084 87	V 2.269 1
25 Mn	2.101 820	2.105 78	1.910 21	Cr 2.070 20
26 Fe	1.936 042	1.939 980	1.756 61	Mn 1.896 43
27 Co	1.788 965	1.792 850	1.620 79	Fe 1.756 61
29 Cu	1.540 562	1.544 390	1.392 218	Ni 1.488 07
42 Mo	0.709 300	0.713 590	0.632 288	Nb 0.652 98

$$x_{\psi\theta}^{\Omega} = \frac{1}{2\mu}\frac{\sin^2\theta - \sin^2\psi}{\sin\theta\cos\psi} \quad (9)$$

$$x_{\psi\theta}^{\chi} = \frac{1}{2\mu}\sin\theta\cos\psi \quad (10)$$

$$x_{\beta\theta}^{\chi_m} = \frac{1}{2\mu}\cos\beta\left(1 - \cot^2\theta\right) \quad (11)$$

9.3 *Filters*—Filters may be used to suppress K_β peak interference and fluorescence. A filter material is chosen based on the K_{edge} value, which should lie between the target K_α and K_β wavelength values. See Table 1.

9.4 *Monochromators*—Monochromators(s) may be used to eliminate spectral components including the Kβ and the Kα2 line, although they will reduce the beam intensity and increase measurement time significantly.

9.5 *Modes*—Three modes are described in 9.5.1 – 9.5.3. Each has specific advantages and disadvantages. Some goniometers offer multiple modes.

9.5.1 *Omega Mode*—Also known as iso-inclination, ω, or Ω method. With omega mode, the incident beam and ψ angle(s) remain on the σ_φ-σ_{33} plane. Multiple ψ angles are observed by rotation about the ω, Ω, θ, or $\sigma_{\varphi+90°}$ axis while χ remains equal to zero.

9.5.1.1 *Advantages:*

(1) Keeps experiment two dimensional (2D), which is useful for thin coatings, films, and layers;

(2) Capable of accessing deep grooves perpendicular to axis of rotation;

(3) Using two detectors (if available) simultaneous observation of both Debye ring locations is possible over the recommended complete ψ range; and

(4) Conducive to slit optics and improved particle statistics.

9.5.1.2 *Disadvantages:*

(1) Absorption varies with ψ angle;

(2) The use of single detector systems may require 180° rotation of the sample about the σ_{33} axis to realize the full recommended ψ range while avoiding low incidence angle errors; and

(3) Alignment issues may negate advantages of using two detectors.

9.5.2 *Chi Mode*—Also known as side-inclination or χ method. With ω, Ω, or θ equal to 2θ/2, multiple ψ angles are observed by rotation about the χ or $\sigma_{\varphi+90°}$ axis while χ remains equal to ψ.

9.5.2.1 *Advantages:*

(1) Lorentz-polarization-absorption (LPA) is not affected with varying ψ angle and

(2) Capable of accessing deep grooves parallel to axis of rotation.

9.5.2.2 *Disadvantages:*

(1) Beam spot on sample is pseudo elliptical and spreads appreciably and

(2) Usually requires spot focus and collimators that reduce particle statistics.

9.5.3 *Modified Chi Mode*—With modified chi mode, the source positioning, sample positioning, and axis of rotation are the same as omega mode. The detector positions, however, are rotated 90° about the incident beam creating a fixed χ offset

TABLE 2 Commonly Used Target, Plane, and 2θ Combinations

Target	{hkl}	Alloy	2θ	½ $s_2^{\{hkl\}}$	$s_1^{\{hkl\}}$	$X_{\psi\theta}^{\Omega}$ and $X_{\psi\theta}^{\chi}$ ψ = 0°	$X_{\psi\theta}^{\Omega}$ ψ = 45°	$X_{\psi\theta}^{\chi}$ ψ = 60°
			[degrees]	[10^{-6} MPa^{-1}]			[μm]	
				Ferritic and Martensitic Steels—BCC				
Cr Kα	{211}	–	156.07 (1)	5.76 (7) 6.35 (HS-784) (0.73 %C)	-1.25 (7) -1.48 (HS-784) (0.73 %C)	5.60	3.78	2.80
		4340 (50 Rc)	156.0 (8)	5.92 (8)	–	5.46	3.69	2.73
		SAE 52100 100Cr6	~156	5.7504 (7)	-1.327 (7)	5.58	3.77	2.79
		M50	~156	5.577 (7)	-1.287 (7)	4.98	3.36	2.49
		M50-Nil		5.4645 (7)	-1.261 (7)	4.37	2.95	2.18
Fe Kα	{220}	–	145.54 (1)	5.63 (HS-784) (0.39 %C)	-1.32 (HS-784) (0.39 %C)	8.65	5.55	4.33
Co Kα	{310}	–	161.32 (1)	6.98 (7) 7.48 (HS-784) (0.73 %C)	-1.66 (7) -1.84 (HS-784) (0.73 %C)	11.14	7.67	5.57
	{220}	–	123.9 (7)	5.76 (7)	-1.25 (7)	9.97	5.05	4.98
	{211}	–	99.7 (7)	5.76 (7)	-1.25 (7)	8.63	1.76	4.32
Mo Kα	{732+651} (1)	–	153.88 (7)	6.05 (7)	-1.34 (7)	16.88	11.30	8.44
Ti Kα	{200}	–	146.99 (1)	–	–	16.40	10.97	8.20
				Austenitic Steels—FCC				
Mn Kα	{311}	–	152.26 (1)	6.98 (7)	-1.87 (7)	7.02	4.66	3.51
Cr Kβ	{311}	–	148.74 (1)	6.98 (7)	-1.87 (7)	5.50	3.57	2.75
Cr Kα	{220}	–	128.84 (1) 128 ± 1 (HS-784)	6.05 (7)	-1.56 (7)	5.16	2.81	2.58
		304 SS	129.0 (8)	7.18 (8)	–	5.06	2.76	2.53
Cu Kα	{420}	–	147.28 (1) 150 ± 3 (HS-784)			1.94	1.27	0.97
		Incoloy 800	147.0	6.75 (8)		2.90	1.87	1.45
Cu Kα	{331}	–	138.53 (1) 146 (HS-784)			1.92	1.23	0.96
Mo Kα	{884}	–	150.87 (1)			16.29	10.74	8.15

(χ_m). Conflicting nomenclature may be found in literature with regard to axis names. For example, the χ and ω names may be reversed such that multiple angles are observed by rotation about the χ axis. Since modified chi mode is typically used by omega mode diffractometers with detector positioning rotated 90° about the incident beam, omega axis labeling is used for consistency.

9.5.3.1 *Advantage*—Capable of accessing deep grooves parallel to axis of rotation.

9.5.3.2 *Disadvantages:*

(1) Values τ_{12} and τ_{13} cannot be resolved (see 5.4) and

(2) Values τ_{23} and σ_{11} cannot be resolved (see 5.4).

10. Calibration and Standardization

10.1 Instrument alignment can be verified with Test Method E915 by the measurement of a stress-free powder.

10.2 Additionally, a nonzero known residual stress proficiency reference sample should be measured to verify that hardware and software are working correctly.

NOTE 1—No national reference sample exists other than a stress-free sample. It is recommended that round robin methodologies be used to determine the residual stress values of such reference samples. Specification DIN EN 15305 provides a methodology for creating a stress-reference specimen.

11. Procedure

11.1 Position test specimen for measurement in the goniometer. Ensure that specimen-positioning devices such as clamps do not create an applied load because the XRD method does not differentiate between applied and residual stress but rather measures the summation of the two.

11.2 The angular range over which measurements are carried out is limited by the mode used. Measurements should always be performed over the maximum permissible ψ range. If the range is further limited by specimen geometry, the largest possible range should be used where no shadowing effects occur.

11.2.1 *Iso Inclination*—ψ max = ±45° ($\sin^2\psi = 0.5$). (**9**, p. 121)

11.2.2 *Side Inclination*—ψ max = ±77° ($\sin^2\psi = 0.95$). (**9**, p. 121)

11.2.3 *Modified Chi*—β max = ±78° ($\sin^2\beta = 0.96$). (**1**, p. 179)

11.3 In the case of single detector configurations other than chi mode, the range can be restricted to the positive or negative ψ range depending on the goniometer used. The sample can then be rotated 180° about the σ_{33} axis and remeasured to realize the full ψ range while avoiding low-incident angle errors.

11.4 At least three ψ or β angles are to be used, although seven or more are recommended. When possible, ψ or β angles should be chosen such that they are evenly distributed through the $\sin^2\psi$ or $\sin^2\beta$ range used. For modified chi mode, identical positive and negative angles should be chosen to simplify averaging.

11.5 Collect each profile with sufficient exposure time to ensure accurate intensity information is collected. Random error as a result of counting statistics from insufficient collection times may result in an inaccurate peak position determination.

11.6 For each of the profiles collected, apply the following applicable corrections in the following order:

11.6.1 *Gain Correction*—Multichannel detectors may offer a gain correction intended to correct for intensity variations caused by the detector itself. This is performed by collecting the profile of a sample that is nondiffracting in the observed 2θ region with a similar background intensity.

11.6.2 *Data Smoothing*—Smoothing may be applied, but only with caution, as over smoothing will affect the accuracy of peak position determination. If smoothing is used, Fourier smoothing is recommended since the threshold between major peak contributions and smaller noise frequencies are much more distinguishable in the frequency domain.

11.6.3 *Absorption Correction*—The intensity of a diffracted beam may be subject to a θ-dependent absorption effect causing a distortion of the peak profile. This effect can be compensated for using the following equation (**1**, p. 90):

$$I_{corrected} = \frac{I_{measured}}{1 - \tan\psi\cot\theta\cos\eta} \quad (12)$$

11.6.3.1 *Omega mode absorption correction*—η = 0°.

$$I_{corrected} = \frac{I_{measured}}{(1 - \tan\psi\cot\theta)} \quad (13)$$

11.6.3.2 *Chi mode absorption correction*—η = 90°.

$$I_{corrected} = I_{measured} \quad (14)$$

11.6.3.3 *Modified chi mode absorption correction*

$$I_{corrected} = I_{measured} \quad (15)$$

11.6.4 *Background Correction*—To account for sloping peak backgrounds, choose two reference points on either side of the diffraction profile. This is typically achieved by fitting a selected range within background using a linear least squares regression. The line intensity drawn between these two points is subtracted from the profile giving the peak a level background of zero.

11.6.5 *Lorentz-Polarization Correction*—The intensity of a diffracted beam is subject to additional θ dependent effects known as Lorentzian and polarization effects. This causes a further distortion of the peak profile particularly for wide diffraction peaks at high 2θ angles. These effects can be compensated for using the following equation (**8**, p. 131):

$$I_{corrected} = \frac{I_{actual}}{\left(\frac{1+\cos^2(2\theta)}{\sin^2\theta\cos\theta}\right)} \quad (16)$$

11.6.6 *Modified Lorentz-Polarization Correction*—For broad diffraction peaks at high 2θ angles, the modified Lorentz-polarization correction can result in a more symmetrical peak profile (**8**, p. 463):

$$I_{corrected} = \frac{I_{actual}}{\left(\frac{1+\cos^2(2\theta)}{\sin^2\theta}\right)} \quad (17)$$

12. Calculation and Interpretation of Results

12.1 The position of the corrected XRD peak profiles should be determined using an appropriate method. Historically, popular practices such as stripping the $K_{\alpha2}$ peak and then using a parabolic peak fit to the top 20 % of the peak profile have been shown to be subject to significant errors (**10**, pp. 103-111). The parabolic fit is capable of producing satisfactory results for standards such as Test Method E915 for the measurement of fine-grained, isotropic materials; however, its use for anisotropic bearing steels can be subject to additional errors and should be used with caution.

12.2 The profiles may either be in 2θ or channel-versus-intensity format.

12.3 To ensure accurate peak position determination, the entire peak profile including background should be included. Peak truncation caused by collection over an insufficient 2θ range has been shown to cause inaccurate peak position determination without the use of advanced numerical methods (**11**, pp. 524-525). Generally, the detector width should be three times the FWHM value.

12.4 *Selection of Peak Position Determination Method*—There are a number of methods to determine the position of the XRD peak. If a function is used, the function that best describes the corrected peak shape should be used when using position-sensitive detectors assuming the peak is approximately centered in the detector window. Commonly used peak functions are listed in Table 3.

12.4.1 Many factors affect peak shape including material properties and goniometer configuration. Fig. 14 shows an example of incident beam size effect on peak shape in which an increasing incident beam size results in a transition from a Pearson VII profile with a distinguishable $K_{\alpha1}$ $K_{\alpha2}$ contribution to a well overlapped Gaussian profile.

12.5 Relative peak positions are usually determined using the absolute or cross-correlation method. If the detectors are not calibrated for actual 2θ positioning, an assumed stress-free 2θ value may be used if periodically checked for accuracy. Note, however, that stress-free 2θ values can significantly change with depth in case-hardened steels.

12.5.1 *Cross-Correlation Method (DIN EN 15305)*—Diffraction angles are determined relative to a chosen reference peak. For instance, in omega or chi mode, the 2θ position is given by:

TABLE 3 Peak Distribution Functions

Name	Equation	Values a = Intensity b = Center
Gaussian	$f(x) = ae^{-\frac{(x-b)^2}{2c^2}}$	c = Peak width constant
Pearson VII	$f(x) = a\left\{1+\frac{(x-b)^2}{mc^2}\right\}^{-m}$	c = Peak width constant m = Tail curvature constant
Cauchy	$f(x) = a\left\{1+\frac{(x-b)^2}{c^2}\right\}$	c = Peak width constant
Generalized Fermi function	$f(x) = \frac{A}{e^{-q(x-b)}+e^{r(x-b)}}$	q,r = Left and right side peak shape constants (For symmetrical peak, $q = r$) A = Intensity × 2
Parabolic	$f(x) = -c(x-b)^2+a$	c = Peak width constant

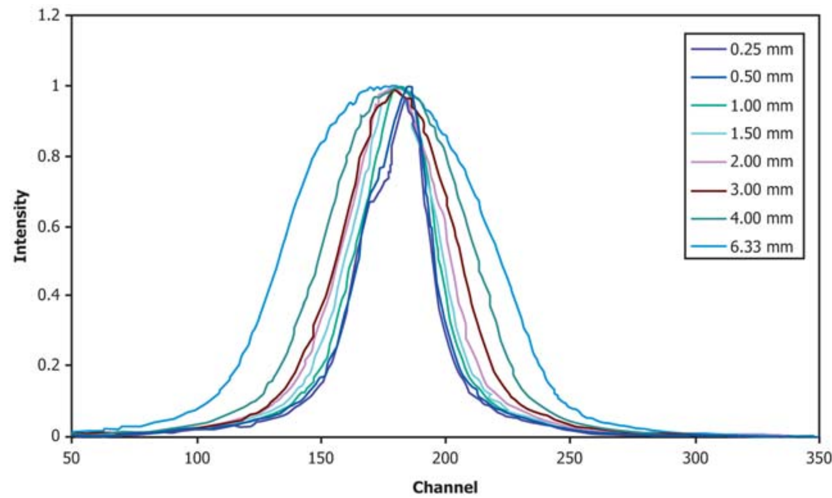

FIG. 14 Example of Incident Beam Size Effect on Peak Shape

$$2\theta_\psi = 2\theta_{ref} + \delta_\psi \quad (18)$$

12.5.1.1 It is recommended to use the strongest peak in the series for the reference peak. The shift is calculated as the value for which the cross section between the actual and reference profile becomes maximal.

$$F(\delta_\psi) = \int I_{ref}(2\theta) I_\psi(2\theta - \delta_\psi) d(2\theta) = \max \quad (19)$$

12.5.1.2 If texture effects are present, the use of cross correlation may cause larger errors than other methods.

12.5.2 *Absolute Method*—Diffraction angles are determined relative to each detector.

12.6 The 2θ values are converted to d spacing using Bragg's law.

$$n\lambda_{K\alpha 1} = 2d_{\varphi\psi}^{\{hkl\}} \sin\theta_{\varphi\psi K\alpha 1}^{\{hkl\}} \quad (20)$$

12.7 The measurement d_o value shall be determined for the calculation of strain.

12.7.1 d_o *Omega and Chi Mode*—When using the plane stress model, there is a negligible error for the substitution of d_o with $d_\perp \psi = 0$ (HS-784). When d versus $\sin^2\psi$ plots exhibit large oscillations or random deviations, an elliptical regression of the data using Eq 21 may produce a more accurate estimate of $d_\perp$ (HS-784).

$$d_{\varphi\psi}^{\{hkl\}} = A \sin^2\psi + B\sin(2\psi) + d_\perp \quad (21)$$

where:

A and B = regression variables.

12.7.1.1 In the case of single-detector omega mode in which software does not support overlapping of separate positive and negative ψ range collections, and such oscillations or deviations are present, a linear regression may be performed separately for the positive and negative range to determine each $d_\perp$ value, respectively.

$$d_{\varphi\psi}^{\{hkl\}} = A \sin^2\psi + d_\perp \quad (22)$$

where:

A = regression variable.

12.7.2 d_o *Modified Chi Mode*—When using the plane stress model, there is a negligible error for the substitution of d_o with $d_\perp \beta = 0$ (HS-784). When d versus $\sin^2\beta$ plots exhibit large

oscillations or random deviations, an elliptical regression of the data may produce a more accurate estimate of $d_\perp$.

$$d^{\{hkl\}}_{\beta\chi_m} = A\ \sin^2\beta + B\sin\beta + C\sin(2\beta) + D\cos\beta + E \tag{23}$$

where:

$$d_\perp = D + E \quad (\text{see X1.2})$$

A, B, C and D = regression values.

12.8 *Strain Calculation*—The strain value for each data point is determined using one of the following methods.

12.8.1 *Linear Variation*—Also known as Cauchy or engineering strain.

$$\varepsilon^{\{hkl\}}_{\varphi\psi} = \frac{d_{\varphi\psi} - d_o}{d_o} = \frac{\Delta d}{d} = \frac{\sin\theta_o}{\sin\theta_{\varphi\psi}} - 1 \tag{24}$$

12.8.2 *Differentiating Bragg's Law:*

$$\varepsilon^{\{hkl\}}_{\varphi\psi} = -\frac{\cot\theta\Delta 2\theta}{2} \tag{25}$$

12.8.3 *True Strain Definition:*

$$\varepsilon^{\{hkl\}}_{\varphi\psi} = \ln\left[\frac{d_{\varphi\psi}}{d_o}\right] = \ln\left[\frac{\sin\theta_o}{\sin\theta_{\varphi\psi}}\right] \tag{26}$$

12.9 *Stress Calculation (Omega and Chi Mode):*

12.9.1 The ε versus $\sin^2\psi$ data is fit using Eq 4 and the values for σ_{11}, τ_{13}, and C may then be determined.

12.9.2 In the case of single-detector configurations other than chi mode in which software does not support overlapping of separate positive and negative ψ range collections, a linear regression may be performed separately for both the positive and negative ranges using Eq 27. The two resulting σ_{11} values may then be averaged. This method should be used with caution as it ignores the shear stresses that may be present.

$$\varepsilon^{\{hkl\}}_{\varphi\psi} = \frac{1}{2}s_2^{\{hkl\}}\left[\sigma_{11}\sin^2\psi\right] + C \tag{27}$$

12.10 *Stress Calculation (Modified Chi Mode):*

12.10.1 The ε versus $\sin^2\beta$ data is fit using Eq 28 and the values for σ_{11}, C, and D may then be determined.

$$\varepsilon^{\{hkl\}}_{\beta\chi_m} = \frac{1}{2}s_2^{\{hkl\}}\left[\sigma_{11}\sin^2\beta\ \cos^2\chi_m + D\right] + C \tag{28}$$

where:

$$\chi_m = \frac{180° - 2\theta_{\beta\chi_m}}{2}$$

12.10.2 In the case of single-detector configurations other than chi mode in which software does not support overlapping of separate positive and negative β range collections, a linear regression may be performed separately for both the positive and negative ranges. The two resulting σ_{11} values may then be averaged. This method should be used with caution as it ignores the shear stresses that may be present.

12.11 *Stress Error Calculation*—Various sources may contribute to the error in stress measurement values and can be considered statistical or systematic.

12.11.1 Statistical errors include detector-counting statistics and the repeatability of the peak position determination method. Neglecting statistical error, a repetition of a measurement will always give the same result.

12.11.2 Systematic errors include goniometer alignment and the errors in parameters used for the measuring and evaluation procedure. The systematic errors of a single measurement cannot be determined.

12.11.3 Ideally, the error of all sources should be considered and combined through error propagation, although this is not always possible or practical. The linear or elliptical regression errors of the d versus $\sin^2\psi$ or d versus $\sin^2\beta$ data provide only an indication of measurement error. The error in peak position determination as well as X-ray elastic constant(s) may also be included through propagation.

12.12 *Gradient Correction*—Also known as transparency correction. Differences in effective layer thickness with orientation and target-plane combinations can affect the measured stress of samples when a stress gradient versus depth is present. The gradient correction determines the true 2θ values for recalculation. (See HS-784, p. 75 for procedure.)

12.13 *Material Removal Correction*—Material removal via electropolishing does not impart any stress in the sample; however, relaxation or redistribution of residual stresses in the component may occur if a stressed layer is removed. There are models available for simple geometries such as a solid cylinder, hollow cylinder, and infinite flat plate for determining what the stresses were before material removal (see HS-784, p. 76). A spherical model is also available based on the cylindrical model (**12**, p. 1372). These models should be used with caution as they assume a material removal from entire surfaces, which is frequently not the case. If finite element model solutions are available, these should be used for best accuracy.

12.14 *Relaxation as a Result of Sectioning*—It is commonly necessary to section samples to gain access to the measurement location thus potentially altering the stress state of the sample. It is advantageous to monitor the change in stress using strain gauge(s) in the intended direction of measurement. Relaxation through a section may be estimated by placing a strain gauge on either side of certain geometries. The relaxation profile between the two gauges may be considered linear or calculated via other analytical or numerical methods, assuming the material properties remain consistent throughout the section and radial stress is disregarded (see HS-784, p. 43). XRD measurements before and after sectioning are also an acceptable means for approximating relaxation. If an accessible area is adjacent to the desired measurement area, then before and after XRD measurements should determine if relaxation has occurred.

13. Report

13.1 Reported data may include the following main items to ensure that sufficient information is available for comparison of results as well as record-keeping purposes.

13.1.1 *General Information:*

13.1.1.1 Specify the operator(s) who performed all aspects of the measurement;

13.1.1.2 Sample identification such as part number, lot number, and so forth;

13.1.1.3 Specifications used for sample preparation, measurement, and reference to result requirements; and

13.1.1.4 Measurement location and direction.

13.1.2 *Results*—The following values are placed in a table using international standardized units (MPa, mm) or Imperial units (ksi, inches) or both. In the case of stress profiles, graphs should also be included displaying SI or U.S. customary units or both.

13.1.2.1 Normal and shear stress values (if available) including errors and direction of measurement relative to the sample reference frame;

13.1.2.2 FWHM values (if required or available) including errors. In the case of two detector setups, the average values may also be included if required; and

13.1.2.3 Integrated intensity ratio values if required or available (see 14.2.1).

13.1.3 *Verification of Equipment Used:*

13.1.3.1 Current Test Method E915 results including date;

13.1.3.2 Current measurement results of stress free standard other than 13.1.3.1 (that is, single daily measurement); and

13.1.3.3 Current measurement results of nonzero known residual stress proficiency reference sample if available.

13.1.4 *Measurement Parameters:*

13.1.4.1 Equipment used including manufacturer and model;

13.1.4.2 Goniometer mode;

13.1.4.3 Goniometer radius;

13.1.4.4 Software and version used for goniometer control, data acquisition, and data processing;

13.1.4.5 Target and wavelength used, for example, Cr $K\alpha_1$ 2.289 70 [Angstroms];

13.1.4.6 Target power used, for example, 30.00 mA × 30.00 kV = 900 W = 69 % (percent of maximum power);

13.1.4.7 Filters used and whether the filter is located between the source and sample or sample and detector;

13.1.4.8 Sample material, for example, M50;

13.1.4.9 Miller indices of crystallographic plane used, for example, {211};

13.1.4.10 The d_o Bragg angle in degrees;

13.1.4.11 Detector type used;

13.1.4.12 The 2θ region scanned;

13.1.4.13 Step size or channel size in degrees 2θ;

13.1.4.14 Counting time per step for single-channel detectors or exposure time × number of exposures for linear array detector;

13.1.4.15 The β angles used in degrees;

13.1.4.16 The ψ angles used in degrees;

13.1.4.17 The φ angles used in degrees for triaxial measurement;

13.1.4.18 Primary and secondary aperture size;

13.1.4.19 *X-ray elastic constant ½ S_2*—Include S_1 for triaxial measurement;

13.1.4.20 *Data smoothing*—If used specify method/formula used; and

13.1.4.21 Estimated depth of penetration at $\psi = 0°$ and $I = 0.63\ I_o$.

14. Precision and Bias

NOTE 2—The precision of this method will be dependent upon the sources of error described in this section. The repeatability standard deviation has been experimentally determined for fine-grained isotropic materials. The reproducibility of this test method is being determined and both will be available on or before May 2017.

14.1 *Uncertainty in Peak Fitting*—The collected peak profile is a summation of multiple overlapping peaks. Therefore, not properly accounting for all contributions will affect the accuracy of deconvoluting individual contributions using profile regression. Possible deviations include the following:

14.1.1 *Peak Asymmetry*—This is commonly observed in bearing steel materials. Possible sources of asymmetry include dislocation effects, separation of peaks as a result of slight tetragonalities in cubic materials, and incomplete heat treatment causing a mixture of ferrite and martensite.

14.1.2 *Interfering Peak(s)*—Diffraction peaks free of interfering peaks from the measured phase are typically used. The presence of other phases such as carbides may create interfering peaks.

14.1.3 *Counting Statistics*—Random error as a result of counting statistics may result from failure to take sufficient time during the measurement to obtain accurate intensity information and, thus, to determine accurately the diffraction peak positions. Methods are available (HS-784) for estimating the standard deviation of the measured stress as a result of the errors involved in counting and curve fitting to determine peak positions.

14.2 *Uncertainty in d Versus $\sin^2\psi$ or $\sin^2\beta$ Fitting*—There are many possible sources of error in the d versus $\sin^2\psi$ or $\sin^2\beta$ plot. Some of these errors may create an elliptical offset causing an apparent shear influence, while others create oscillatory or seemingly random patterns. Deviations often become more apparent at lower σ_{11} values because of the lower d-spacing axis scaling. Distinguishing between sources of error can be difficult and multiple influences may overlap. Some possible sources are listed in the following.

14.2.1 *Texture*—A nonrandom coherent domain orientation distribution is found in all bearing materials in varying degrees. Texture may be manifested by a significant change in peak intensity versus orientation as well as oscillatory $\sin^2\psi$ distributions. The degree of texture observed in a measurement is indicated by the peak integrated intensity ratio (Eq 29).

$$I.R.^{\{hkl\}} = \frac{I_{max}}{I_{min}} \quad (29)$$

14.2.1.1 Intensity ratios above 1.6 may require corrective actions that include the following:

(1) Different hkl plane—It has been shown that some *hkl* planes are more susceptible to nonelliptical $\sin^2\psi$ distributions than others for cubic materials (**12**, pp. 899-906) and

(2) Maximize ψ tilt—It has been suggested that linearization of the d versus $\sin^2\psi$ distribution may be achieved by maximizing the ψ tilt range (**1**, p. 189).

14.2.2 *Stress Gradient*—A significant stress gradient within the diffracted volume will affect the dependence of measured strain with incident beam orientation because of a difference in volume penetration. In chi and omega mode, large gradients may be indicated by a curved d versus $\sin^2\psi$ distribution.

Unlike curvatures caused by shear stress, the curvatures caused by a stress gradient bend in the same direction for the positive and negative ψ range (see Fig. 15) (**1**, p. 181). Corrections are available for the stress gradient effect (HS-784, p. 75).

14.2.3 *Large Grain Size*—For a given homogeneous volume, a larger grain size will reduce the number of grains available for diffraction at a given orientation. This is often associated with random deviations in the $\sin^2\psi$ or $\sin^2\beta$ plot. Intensity ratios above 1.6 may require corrective actions that include the following:

14.2.3.1 *Different hkl plane*—It has been shown that some *hkl* planes are more susceptible to nonelliptical $\sin^2\psi$ distributions than others for cubic materials (**13**, pp. 899-906). The selection of a high-multiplicity *hkl* plane may also reduce the effects of large grain size.

14.2.3.2 *Oscillation(s)*—The φ and β oscillations as well as sample translation may be introduced to minimize the effects of large grains (**14**).

14.2.3.3 *Increase aperture size*—Where possible, the use of a larger aperture will increase the number of grains sampled and minimize the effects of large grain size.

14.2.3.4 *Increase number of tilts and range*—Increasing the number of ψ tilts and the ψ tilt range can also reduce errors caused by large grain size.

14.2.3.5 *Deeper penetrating radiation*—A deeper penetration may increase the number of grains sampled and reduce the effects of large grain size.

14.2.4 *Temperature Gradient*—Changes in sample temperature will cause a change in strain according to the material coefficient of thermal expansion. If the sample material is gradually heated or cooled during measurement, a change in strain will occur. For example, the air in a goniometer enclosure may be warmer than the outside ambient air causing the sample to warm up gradually when placed in the enclosure for measurement. Fig. 16 shows *d*-spacing deviations caused by a 5°C increase in temperature during measurement. The rate of sample temperature change will depend on its thermal conductivity.

14.2.5 *Stability of Residual Stress/Strain*—Residual stresses may cause the strain to change over time through creep mechanisms. The strain rate of change is largest in the primary stage after the stresses are created or altered and will slow over time with increasing strain. Larger strain rates may cause a significant change in strain over the course of the measurement. The effects of aging may also contribute to the stability of residual stress over time.

14.2.6 *Plastic Deformation*—Oscillatory $\sin^2\psi$ or $\sin^2\beta$ plots may occur as a result of plastic deformation (**1**, p. 400).

14.3 *Maximum Acceptable Errors:*

14.3.1 Intensity ratio shall not exceed 3.0. Corrective actions may be required if the intensity ratio exceeds 1.6.

14.3.2 *Stress Values*—Alternatively, strain values may be used. This avoids error as a result of the selection of inappropriate elastic constants.

14.3.2.1 Normal stress error not to exceed 10 % of the normal stress value or 35 MPa, whichever is larger. Corrective actions may be required if error exceeds 20 MPa.

14.3.2.2 Normal strain error not to exceed 10 % of the normal strain value or 250 ppm, whichever is larger. Corrective actions may be required if the error exceeds 150 ppm.

14.3.2.3 Shear stress errors not to exceed 10 % of the shear stress value or 35 MPa, whichever is larger. Corrective actions may be required if the error exceeds 20 MPa.

14.3.2.4 Shear strain errors not to exceed 10 % of the shear strain value or 125 ppm, whichever is larger. Corrective actions may be required if the error exceeds 75 ppm.

14.4 *Uncertainty in Stress Values*—Sources of experimental error in the residual stress measurement result may include the following:

14.4.1 *X-Ray Elastic Constant(s)*—Factors affecting Young's modulus will also affect the X-ray elastic constants. X-ray elastic constants may be determined with Test Method E1426. Some examples of X-ray elastic constant influences include the following:

14.4.1.1 *Stability of residual stress/strain*—Material instabilities such as creep and aging may influence the stress-strain relationship over time.

14.4.1.2 *Chemistry*—Material chemistry can have a large influence on X-ray elastic constants. For example, in case-hardened steels, a carbon gradient versus depth can cause a significant material properties gradient with depth.

14.4.1.3 *Grain structure*—In martensitic steels, two structures are commonly observed: "lath" and "plate" martensite

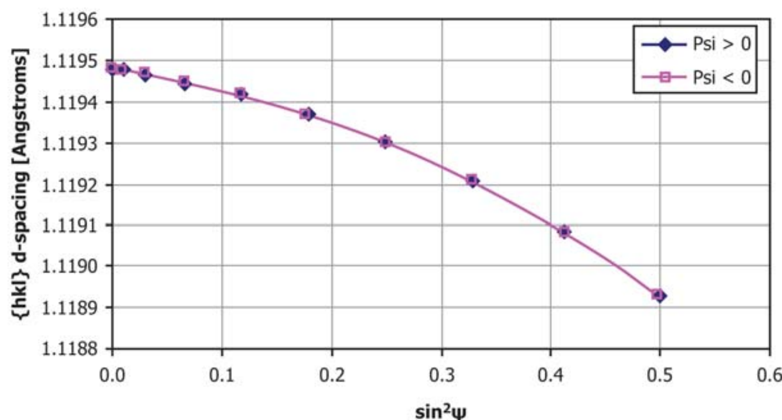

FIG. 15 Sample *d* Versus $\sin^2\psi$ Dataset with Large Stress Gradient

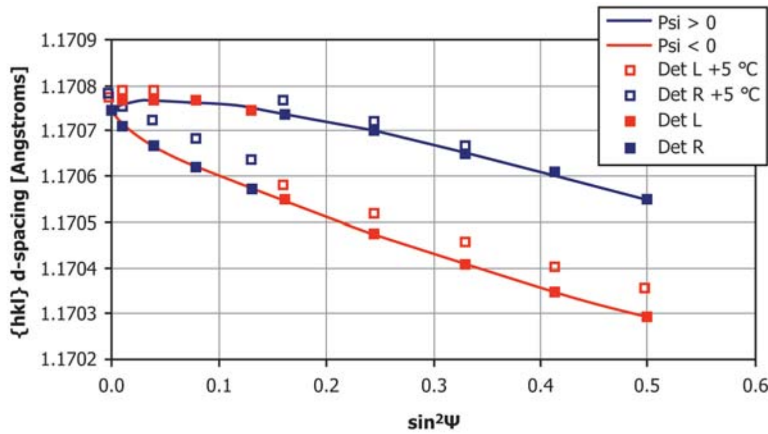

FIG. 16 Simulated Two Detector Omega Mode $\sin^2\psi$ Offset for 5°C Increase during Measurement where σ_{11} = -100 MPa, τ_{13} = +20 MPa, and α_L = 11 × 10^{-6} mm/mm/°C (α_L Applied to $d_o^{\{hkl\}}$ Value)

(**15**). The percentage of each structure is largely dependent on the carbon content and where the carbon is concentrated, that is, in solution/in carbides.

14.4.2 *Sample Alignment*—The sample measurement location shall remain aligned with the goniometer center of rotation. This is especially true for curved surfaces where measurement of misaligned samples can result in *d*-spacing offsets that appear to be stress component influences.

14.4.3 *Sample Curvature*—Sample curvature should not exceed limits specified in 9.1.2.

14.4.4 *Surface Condition*—Sample surface should be prepared in accordance with 8.2.

14.4.5 *X-Ray Optics*—X-ray optics should be used according to the manufacturer's specifications.

14.4.6 *Errors in Peak Fitting*—See 14.1.

14.4.7 *Errors in $\sin^2\psi$ or $\sin^2\beta$ Fitting*—See 14.2.

15. Keywords

15.1 bearing; residual stress; X-ray diffraction; XRD

APPENDIX

(Nonmandatory Information)

X1. MODIFIED χ CALCULATION

X1.1 The values, ψ and φ, are converted to β and χ reference using Eq 5 and 6.

$$\psi = \arccos(\cos\beta\cos\chi_m) \qquad (5)$$

$$\varphi = \arccos\left(\frac{\sin\beta\cos\chi_m}{\sin\psi}\right) \qquad (6)$$

X1.2 Eq 5 and 6 are applied to each term in Eq 2.

$$\varepsilon_{\varphi\psi}^{\{hkl\}} = \frac{1}{2}s_2^{\{hkl\}}\left[\sigma_{11}\cos^2\varphi\sin^2\psi + \sigma_{22}\sin^2\varphi\sin^2\psi + \sigma_{33}\cos^2\psi\right]$$
$$+\frac{1}{2}s_2^{\{hkl\}}\left[\tau_{12}\sin(2\varphi)\sin^2\psi + \tau_{13}\cos\varphi\sin(2\psi) + \tau_{23}\sin\varphi\sin(2\psi)\right]$$
$$+s_1^{\{hkl\}}\left[\sigma_{11}+\sigma_{22}+\sigma_{33}\right] \qquad (2)$$

$\sigma_{11}\cos^2\varphi\sin^2\psi$

$= \sigma_{11}\frac{\sin^2\beta\cos^2\chi_m}{\sin^2\psi}\sin^2\psi$

$= \sigma_{11}\sin^2\beta\cos^2\chi_m$

$\sigma_{22}\sin^2\varphi\sin^2\psi$

$= \sigma_{22}\sin^2\left[\arccos\left(\frac{\sin\beta\cos\chi_m}{\sin^2\psi}\right)\right]\sin^2\psi$

$\because \sin^2(\arccos(x)) = 1 - x^2$

$= \sigma_{22}\left(1-\frac{\sin^2\beta\cos^2\chi_m}{\sin^2\psi}\right)\sin^2\psi$

$= \sigma_{22}(\sin^2\psi - \sin^2\beta\cos^2\chi_m)$

$= \sigma_{22}(\sin^2[\arccos(\cos\beta\cos\chi_m)] - \sin^2\beta\cos^2\chi_m)$

$\because \sin^2(\arccos(x)) = 1 - x^2$

$= \sigma_{22}(1-\cos^2\beta\cos\chi_m - \sin^2\beta\cos^2\chi_m)$

$= \sigma_{22}(1-\cos^2 x(\cos^2\beta+\sin^2\beta))$

$\because \cos^2 x + \sin^2 x = 1$

$= \sigma_{22}(1-\cos^2\chi_m)$

$\because\ 1-\cos^2 x=\sin^2 x$

$=\sigma_{22}\sin^2\chi_m$

$\sigma_{33}\cos^2\psi$

$=\sigma_{33}\cos^2(\arccos(\cos\beta\cos\chi_m))$

$\because\ \cos^2(\arccos x)=x^2$

$=\sigma_{33}\cos^2\beta\cos^2\chi_m$

$\tau_{12}\sin(2\varphi)\sin^2\psi$

$$=\tau_{12}\sin\left(2\arccos\left(\frac{\sin\beta\cos\chi_m}{\sin\psi}\right)\right)\sin^2\psi$$

$\because\sin(2\arccos x)=2x\sqrt{1-x^2}$

$$=\tau_{12}\frac{2\sin\beta\cos\chi_m}{\sin\psi}\sqrt{1-\frac{\sin^2\beta\cos^2\chi_m}{\sin^2\psi}}\sin^2\psi$$

$$=\tau_{12}2\sin\beta\cos\chi_m\sin\psi\sqrt{1-\frac{\sin^2\beta\cos^2\chi_m}{\sin^2\psi}}$$

$$=\tau_{12}2\sin\beta\cos\chi_m\sin(\arccos(\cos\beta\cos\chi_m))\sqrt{1-\frac{\sin^2\beta\cos^2\chi_m}{\sin^2(\arccos(\cos\beta\cos\chi_m))}}$$

$\because\sin(\arccos x)=\sqrt{1-x^2}$ and $\sin^2(\arccos x)=1-x^2$

$$=\tau_{12}2\sin\beta\cos\chi_m\sqrt{1-\cos^2\beta\cos^2\chi_m}\sqrt{1-\frac{\sin^2\beta\cos^2\chi_m}{1-\cos^2\beta\cos^2\chi_m}}$$

$$=\tau_{12}2\sin\beta\cos\chi_m\sqrt{1-\cos^2\beta\cos^2\chi_m-\frac{(1-\cos^2\beta\cos^2\chi_m)(\sin^2\beta\cos^2\chi_m)}{1-\cos^2\beta\cos^2\chi_m}}$$

$$=\tau_{12}2\sin\beta\cos\chi_m\sqrt{1-\cos^2\beta\cos^2\chi_m-\sin^2\beta\cos^2\chi_m}$$

$$=\tau_{12}2\sin\beta\cos\chi_m\sqrt{1-\cos^2\chi_m(\cos^2\beta+\sin^2\beta)}$$

$\because\ \cos^2 x+\sin^2 x=1$

$$=\tau_{12}2\sin\beta\cos\chi_m\sqrt{1-\cos^2\chi_m}$$

$\because\ 1-\cos^2 x=\sin^2 x$

$=\tau_{12}2\sin\beta\cos\chi_m\sin\chi_m$

$\because\cos x\sin x=\frac{1}{2}\sin(2x)$

$=\tau_{12}2\sin\beta\sin(2\chi_m)$

$\tau_{13}\cos\varphi\sin(2\psi)$

$$=\tau_{13}\cos\left(\arccos\left(\frac{\sin\beta\cos\chi_m}{\sin\psi}\right)\right)\sin(2\psi)$$

$$=\tau_{13}\frac{\sin\beta\cos\chi_m}{\sin\psi}\sin(2\psi)$$

$\because\ \frac{\sin(2x)}{\sin x}=2\cos x$

$=\tau_{13}2\sin\beta\cos\chi_m\cos\psi$

$=\tau_{13}2\sin\beta\cos\chi_m\cos(\arccos(\cos\beta\cos\chi_m))$

$=\tau_{13}2\sin\beta\cos\beta\cos^2\chi_m$

$\because\cos x\sin x=\frac{1}{2}\sin(2x)$

$=\tau_{13}\sin(2\beta)\cos^2\chi_m$

$\tau_{23}\sin\varphi\sin(2\psi)$

$$=\tau_{23}\sin\left(\arccos\left(\frac{\sin\beta\cos\chi_m}{\sin\psi}\right)\right)\sin(2\psi)$$

$\because\sin(\arccos x)=\sqrt{1-x^2}$

$$=\tau_{23}\sqrt{1-\frac{\sin^2\beta\cos^2\chi_m}{\sin^2\psi}}\sin(2\psi)$$

$$=\tau_{23}\sqrt{1-\frac{\sin^2\beta\cos^2\chi_m}{\sin^2(\arccos(\cos\beta\cos\chi_m))}}\sin(2\arccos(\cos\beta\cos\chi_m))$$

$\because\ \sin^2(\arccos x)=1-x^2$ and $\sin(2\arccos x)=2x\sqrt{1-x^2}$

$$=\tau_{23}\sqrt{1-\frac{\sin^2\beta\cos^2\chi_m}{1-\cos^2\beta\cos^2\chi_m}}\,2\cos\beta\cos\chi_m\sqrt{1-\cos^2\beta\cos^2\chi_m}$$

$$=\tau_{23}2\cos\beta\cos\chi_m\sqrt{1-\cos^2\beta\cos^2\chi_m-\frac{(1-\cos^2\beta\cos^2\chi_m)(\sin^2\beta\cos^2\chi_m)}{1-\cos^2\beta\cos^2\chi_m}}$$

$$=\tau_{23}2\cos\beta\cos\chi_m\sqrt{1-\cos^2\beta\cos^2\chi_m-\sin^2\beta\cos^2\chi_m}$$

$$=\tau_{23}2\cos\beta\cos\chi_m\sqrt{1-\cos^2\chi_m(\cos^2\beta+\sin^2\beta)}$$

$\because\ \cos^2 x+\sin^2 x=1$

$$=\tau_{23}2\cos\beta\cos\chi_m\sqrt{1-\cos^2\chi_m}$$

$\because\ 1-\cos^2 x=\sin^2 x$

$=\tau_{23}2\cos\beta\cos\chi_m\sin\chi_m$

$\because\cos x\sin x=\frac{1}{2}\sin(2x)$

$=\tau_{23}2\cos\beta\sin(2\chi_m)$

X1.3 Bringing the terms together we obtain:

$$\varepsilon^{\{hkl\}}_{\beta\chi_m}=\frac{1}{2}s_2^{\{hkl\}}\left[\sigma_{11}\sin^2\beta\cos^2\chi_m+\sigma_{22}\sin^2\chi_m+\sigma_{33}\cos^2\beta\cos^2\chi_m\right]$$
$$+\frac{1}{2}s_2^{\{hkl\}}\left[\tau_{12}\sin\beta\sin(2\chi_m)+\tau_{13}\sin(2\beta)\cos^2\chi_m+\tau_{23}\cos\beta\sin(2\chi_m)\right]$$
$$+s_1^{\{hkl\}}\left[\sigma_{11}+\sigma_{22}+\sigma_{33}\right]\qquad(7)$$

X1.4 *Modified χ $d_\perp$ Calculation*:

X1.4.1 For β = 0, Eq 23 becomes:

$$d^{\{hkl\}}_{\beta=0\chi_m}=A\sin^2 0+B\sin 0+C\sin(2\cdot 0)+D\cos 0+E=D+E$$

Substituting $d^{\{hkl\}}_{\beta=0\chi_m}$ with $d_\perp$:

$$d_\perp=D+E$$

REFERENCES

(1) Hauk, V., *Structural and Residual Stress Analysis by Nondestructive Methods*, Elsevier, Amsterdam, The Netherlands, 1997.

(2) Noyan, I. C. and Cohen, J. B., *Residual Stress Measurement by Diffraction and Interpretation*, Springer-Verlag, 1987.

(3) Londsdale, D. and Doig, P., "The Development of a Transportable X-Ray Diffractometer for Measurement of Stress," in *International Conference on Residual Stresses ICRS2, Elsevier Applied Science*, London and New York, 1989.

(4) Taira, S. and Arima, J., "X-Ray Investigation of Stress Measurement (on the Effect of Roughness of Specimen Surface)," in *Proceedings of the Seventh Japan Congress on Testing Materials*, The Society of Materials Science, 1964.

(5) SEM, *Handbook of Measurement of Residual Stress*, Fairmont Press, 1996.

(6) Dionnet, B., Francois, M., Lebrun, J. L., and Nardou, F., "Influence of Tore Geometry on X-Ray Stress Analysis," in *Proceedings of the Fourth European Conference on Residual Stresses*, Vol 1, France, 1996.

(7) Residual Stress Measurement by X-Ray Diffraction, Schaeffler Group Standard, 2008.

(8) Cullity, B. D., *Elements of X-Ray Diffraction–Second Edition*, Addison-Wesley Publishing Company Inc., Reading, MA, 1978.

(9) Sue, Albert J. and Schajer, Gary S., *Handbook of Residual Stress and Deformation of Steel – Stress Deformation in Coatings*, ASM International, 2002.

(10) Prevey, P., "The Use of Pearson VII Distribution Functions in X-Ray Diffraction Residual Stress Measurement," *Advances in X-Ray Analysis*, Vol 29, 1986.

(11) Belassel, M., Bocher, E., and Pineault, J., "Effect of detector width and peak location technique on residual stress determination in case of work-hardened materials," *Materials Science Forum*, 2006.

(12) Kikuo, M., Nakashima, H., and Tsushima, N., "The Influence of Residual Stress in Radial Direction upon Rolling Contact Fatigue Life," in *Residual Stresses-III, Science and Technology, ICRS3*, H. Fujiwara, T. Abe, and K. Tanaka, Eds., Applied Science, London and New York, 1992.

(13) Behnken, H. and Hauk, V., "The evaluation of residual stresses in textured materials by X- and neutron-rays," in *Residual Stresses-III, Science and Technology, ICRS3*, Vol 2, H. Fujiwara, T. Abe, and K. Tanaka, Eds., Applied Science, London and New York, 1992.

(14) Pineault, J. A. and Brauss, M. E., "Measuring Residual and Applied Stress Using X-ray Diffraction on Materials With Preferred Orientation and Large Grain Size," *Advances in X-Ray Analysis*, Vol 36, 1993.

(15) Parrish, G., *Carburizing: Microstructures and Properties*, ASM International, 1999, p. 108.

ASTM International takes no position respecting the validity of any patent rights asserted in connection with any item mentioned in this standard. Users of this standard are expressly advised that determination of the validity of any such patent rights, and the risk of infringement of such rights, are entirely their own responsibility.

This standard is subject to revision at any time by the responsible technical committee and must be reviewed every five years and if not revised, either reapproved or withdrawn. Your comments are invited either for revision of this standard or for additional standards and should be addressed to ASTM International Headquarters. Your comments will receive careful consideration at a meeting of the responsible technical committee, which you may attend. If you feel that your comments have not received a fair hearing you should make your views known to the ASTM Committee on Standards, at the address shown below.

This standard is copyrighted by ASTM International, 100 Barr Harbor Drive, PO Box C700, West Conshohocken, PA 19428-2959, United States. Individual reprints (single or multiple copies) of this standard may be obtained by contacting ASTM at the above address or at 610-832-9585 (phone), 610-832-9555 (fax), or service@astm.org (e-mail); or through the ASTM website (www.astm.org). Permission rights to photocopy the standard may also be secured from the Copyright Clearance Center, 222 Rosewood Drive, Danvers, MA 01923, Tel: (978) 646-2600; http://www.copyright.com/